

# HIGH COMPRESSIVE STRENGTH 3D PRINTED INFILL BASED ON STRUT-BASED LATTICE STRUCTURE

Rey Farly Garcia\*, Alvin Chua

Mechanical Engineering Department, Gokongwei College of Engineering, De La Salle University, Manila, Philippines

Article history

Received

15 October 2021

Received in revised form

19 December 2021

Accepted

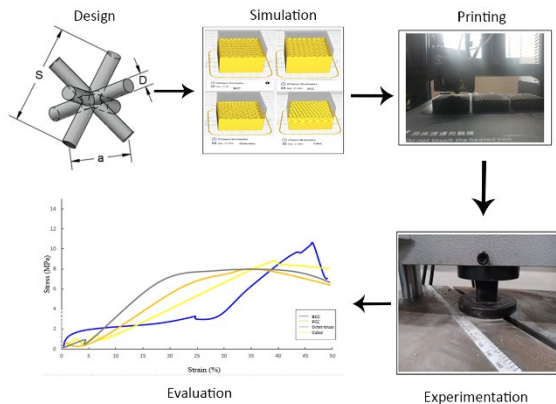
06 February 2022

Published online

30 November 2022

\*Corresponding author  
rey\_garcia@dlsu.edu.ph

## Graphical abstract



## Abstract

In an attempt to make Additive Manufacturing more material-efficient, researchers come across the idea of re-enforcing 3D printed objects by infill pattern modification. In line with this concept, this paper introduces a new innovative infill pattern inspired by a variety of strut-base lattice structures that is stronger and more material-efficient than conventional 3D printing infill. This research provides the design, analysis, and experimental results of the developed 3D printed infills, then compared with a benchmark infill. Three (3) strut-based lattice test samples, namely Body-Centered Cubic (BCC), Face-Centered Cubic (FCC), and Octet-Truss, were designed and 3D printed with an equal amount of material used, then undergo compressive test on Universal Testing Machine. Results showed that BCC, FCC, and Octet-truss infill pattern print has a compressive strength of 11.25 MPa, 8.47 MPa, 7.44 MPa consecutively, while benchmark infill has 9.73 MPa. This data proves that with the same amount of material consumed, the BCC lattice structure infill withstands a compressive load higher than the benchmark infill, which is offered in a 3D printing slicer.

**Keywords:** 3D printing, Additive Manufacturing, Infill, Lattice

© 2022 Penerbit UTM Press. All rights reserved

## 1.0 INTRODUCTION

3D printing through Fuse Deposition Method (FDM) creates objects from any material that can flow and then harden, such as thermoplastic polymers, melted soft metallic material, lab-grown cells, and conductive printable ink. However, 3D printing technology is still focused mainly on the extrusion of thermoplastics [1][2]. The most commonly used in 3D printing thermoplastic filament is Polylactic Acid (PLA) and Acrylonitrile Butadiene Styrene (ABS)[3]. These filaments can print various objects in a wide range of applications, such as printing robotic parts, gadgets accessories, and plastic mold. The creation of 3D models usually started from designing the models using Computer-Aided Design (CAD) software then saved as Stereolithography (STL) format as this format was supported by most of the 3D printing slicing software. Slicing software creates a G-code language that usually is used by 3D printers. 3D printing slicers have different features for the users to customize their

samples before executing printing, such as adjustable object orientation, size reduction and enlargement, the addition of 3D printed support, and weight reduction through infills.

Infill is the printed structure in the interior part of the object. It is done by replacing the solid part of the printing object with a hollowed structure[4]. Slicing software has different choices of infill patterns; it is selected by the user with a configurable amount of volume to be used. Infill patterns and their volume percentage have significantly affected the printed object's physical strength, wherein the more volume that the infills have occupied gives relatively more strength to the object[5]. Higher volume percentage leads to a more resistant print, yet it also consumes more material and prolongs the print time[6], while the use of infills may reduce the physical strength of the printed object due to material reduction. To optimize the printing process, the use of infills to replace solid interior structures is one of the features that the current 3D printing technology has. However, the strength of the infill may vary on its volume

percentage and geometrical structure while a good balance between material consumption and physical strength is key for a material-efficient print. Different studies have found in the literature that analyzed the effect of different infill structures on the printed object. One of those studies were mechanical properties of common infill patterns such as Line, Concentric, and Honeycomb conducted by Farbman and McCoy. They found that infills with hexagonal pattern geometry were stronger and stiffer than infills with rectilinear patterns [7]. Wu, et al. propose a way of combining structural and optimization techniques to generate infill pattern based on the bone structure [8]. This study was based on the principle of Wolff's law of bone, which asserts that bone develops and remodels in response to the stresses applied to it [9]. A bioinspired triply periodic minimal surface (TPMS) infill structure that mimicked the microstructure of Great Spotted Woodpecker's cranial bone was developed and tested by Fan, et. al. The developed structures had shown an improved mechanical property contributed to the designed TPMS surface structure and the wall thickness [10]. Topologically optimized infill structures greatly improve the mechanical properties of a solid object with lesser density as it has the ability to just lay material where it is needed; however, this structure requires complex algorithms that needed more computational time to incorporate in typical 3D printing technologies thus simplification of infill structure makes it accessible for the end users of 3D printers. Moreover, Timothy Scott Chu et al. 2018 proposed the use of lattice structure with symmetrical topologies as an infill which increases material efficiency of 3D printing technology to offer acceptable rigidity comparable to a regular print [11]. A rigid structure based on the lattice pattern shows a great potential which offers high compressive strength due to its synchronization using lesser material.

In this study, three (3) 3D printed infill based on strut-base lattice patterns were analyzed, which aims to increase the mechanical properties of a 3D printed object as well as to increase material efficiency while consuming an equal amount of material with that of benchmark infill. The strut-based cell topologies that have been studied are body-centered cubic (BCC) and face-centered-cubic (FCC), and octet-truss. To evaluate the proposed infill pattern, the researcher compares the compressive strength of benchmark infills with each of the proposed lattice structure infills in a uniform arrangement.

## 2.0 METHODOLOGY

### Lattice Infill Concept

Lattice was defined as a porous structure of repeated cellular units. It has now been studied in different applications for its lightweight and different physical function that can be compared to solid structures [12]. Gibson defines lattice as a cellular material consisting of "an interconnected network of struts or plates" [13]. Ashby also states that the lattice structure is a form of cellular material; it has a unit scale of millimeter or micrometer-scale, contrasting the engineering structures, which are built-in large scales such as trusses and planes [14]. Fabrication of lattice structure has many means, including casting, material extrusion, interlocking, hot-press, and filament winding. After all, lattice fabrication opens up research attention due to the advancement of additive manufacturing techniques [15]. In mathematics, the term "lattice" refers to a group of

points that follows the position of a predetermined pattern [16]. As technology advances within the past decades, the lattice has been incorporated in construction engineering practices such as the adoption of steel lattice for high-rise and special steel structures like power transmission. In [17], an introduction of lattice struts to replace the use of H-shaped steels ribs has overcome its weakness and to reduce the possibility of having an internal gap. It is described as having an alter-connected strut that is connected through nodes from the center, corner, and faces. Its repeated pattern and alter-connection made it structurally stronger compared to a similar density structure made from the same material. Among lattice structures with symmetrical topologies, i.e., having identical parts if were split into halves at its center plane, are Body-centered cubic, Face-centered cubic, and octet-truss. The Body-centered cubic lattice (BCC) is composed of eight lattice points at the corner; all intersect in the points at the center, as shown in Figure 1(a). It has three equal unit cell vectors and three perpendicular interaxial angles. In a unit cell of BCC, the strut fills up 45% of the unit cube. Figure 1(b) illustrates a Face-centered cubic lattice (FCC); it is also composed of eight lattice points at the corner and intersects at the center of each face. In comparison, Octet-truss is composed of eight lattice points at the corner connected at the center points of each face and six face-centered points connected to adjacent points Figure 1(c). According to Deshpande et al. (2001), an Octet-truss has high nodal connectivity of 12, making it a stretch-dominated structure [18]. If it's made out of high strength material, these lattice structures are weight efficient and self-supporting cellular structures which can withstand a considerable amount of stress. Printer slicer software's like Cura® provides many defaults infill patterns to be chosen by the users, such as Grid, Lines, Triangles, Cubic, Tetrahedral Grid, Zig Zag, and many more depending upon the update of the software. But then all of these infill pattern designs are printed horizontally by layers on top of each other, thus creating vertical faces, which as a result, consumes a lot of material to construct. Cubic infill pattern has been chosen as benchmark infill for this study, due to its similarity of structure with in lattice infill and as it is one of the most used by default. As illustrated in Figure 2., it is made up of tilted and stacked cubes. The cubes are oriented to stand on their corners which gives extra strength in the perpendicular direction of the infill and prevents the cubes from being printed with overhanging portions. When viewed in cross-section, this infill seems to be made up of triangles because of its orientation.

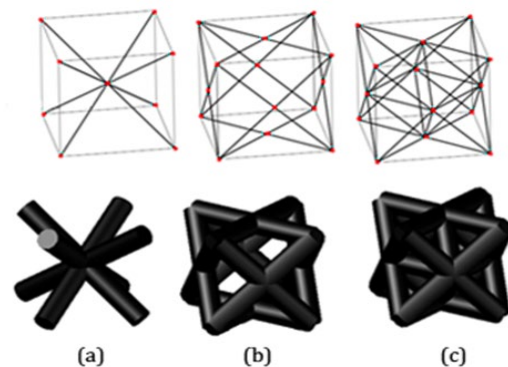


**Figure 1** Strut-based lattice structures; unit cell structure of (a) BCC, (b) FCC, (c) Octet-truss

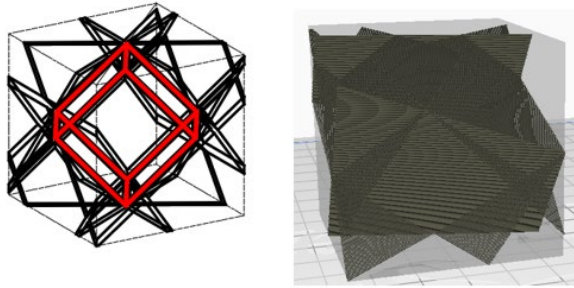


Figure 2 Benchmark infill; (left) unit cell of cubic infill pattern in wireframe view, (right) slice preview of cubic infill pattern in Cura slicing software.

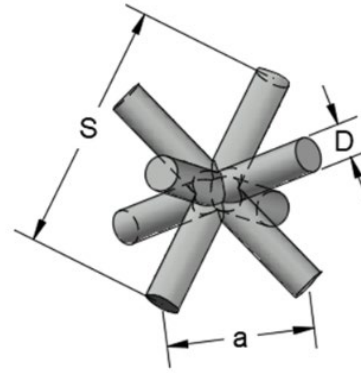


Figure 4 The unit cell of BCC Strut-Base Lattice Structure

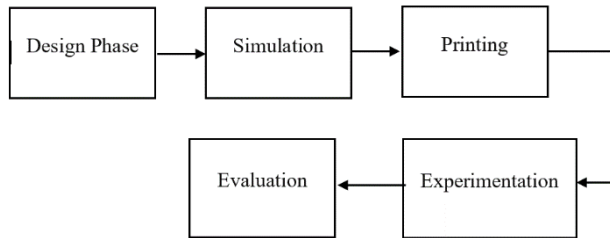


Figure 3 Flow chart of the research methodology

The methodology used in conducting this research was illustrated in the block diagram in Figure 3. The design phase focuses on the calculation of the strut's length and diameter, wherein a unit cell of each strut-based lattice was determined by the volume it occupied using the formula:

$$V_{BCC} = \pi D^2 a \sqrt{3} \tag{1}$$

$$V_{FCC} = \frac{(3\pi D^2 a \sqrt{2})}{2} \tag{2}$$

$$V_{OCTET} = (3\pi D^2 a \sqrt{2}) \tag{3}$$

Since lattice structures are constructed based on the cubical dimension, the formulation for finding the volume of struts was based on cubical dimensions wherein D is strut diameter, S is diagonal of a cube, and a is the side of the cube (see Figure 4). Based on the formula given above, a cubical unit cell of each lattice with an equal strut diameter of 1.25 mm, occupies 30%, 41% and 83% for BCC, FCC and Octet trust consecutively.

In table 1, the dimensions of each unit cells of the proposed lattice structure are shown. Since the cubical testing block was built with a 50.8 mm x 50.8 mm x 50.8 mm dimension, to make each sample uniformed in weight and material cost, the number of cells per sample were transformed into the best fitted figure, this affected the diagonal length and sides of the unit cell while maintaining an equal strut diameter of 1.25 mm. This adjustment made the sample to have different numbers of unit cells per sample resulting to 870 cells, 641 cells, and 266 cells for BCC, FCC and Octet-truss consecutively. Infill percentage was computed as the space to be filled with infills over the total volume of the solid samples or simply the amount of material inside the print. In this work, each sample was printed with a 30% infill percentage. Therefore, the total volume of the infill having 30% infill density is 39329 mm<sup>3</sup> for a 50.8 mm cubical block.

The proposed lattice infill pattern design was constructed using AutoCAD 3D designing software. A representation of the cross-sectional view of the cubical test block with BCC, FCC, and Octet-truss infill patterns was illustrated in figure 5. The differences between the three patterns are challenging to determine at a glance but noticeable in the textures. BCC infill has more expansive space between each cell, while FCC and Octet-truss have narrow gaps due to the front-facing struts. Simulation of both benchmark and proposed infill patterns was conducted in Ultimaker Cura® printer slicing software, wherein the weights of each sample were verified. Weight Verification is necessary to check if the infill density calculation was accurate. Parameters on slicing software are set to have a 2mm wall thickness, 2mm top and bottom thickness, and 100 mm/s printing speed. Based on the simulation, a 50.8

Table 1 Lattice Infill Volume Computation

Lattice Structure	Side (mm)	Diagonal (mm)	Diameter (mm)	Strut Volume (mm <sup>3</sup> )	Total No. of Cell/ Sample	Total Volume of Infill (mm <sup>3</sup> )	Infill Density per 50.8 mm <sup>3</sup>
BCC	5.32	9.2145	1.25	45.209	870.68	39362	30%
FCC	5.89	10.202	1.25	61.302	641.57	39329	30%
Octet-Truss	8.33	14.428	1.25	173.39	266.81	39327	30%

mm cube benchmark with a 30% infill percentage weighs 63 g. Samples with proposed infills need to be self-supporting to avoid complications with the default infill of slicing software, set in 0% infill density. Since lattice structures are not programmed in the slicing software, slicing the testing samples with the proposed infill pattern will create vertical supports by default due to the 45-degree overhanging angle of the strut of lattice structures. So, the default setting of 45-degree overhanging angle support was changed into a 90-degree to avoid printing vertical support that will use unnecessary materials. For the benchmark infill (cubic), it was set in the slicing software with 30% infill density equivalent to the volume density of the proposed infill pattern

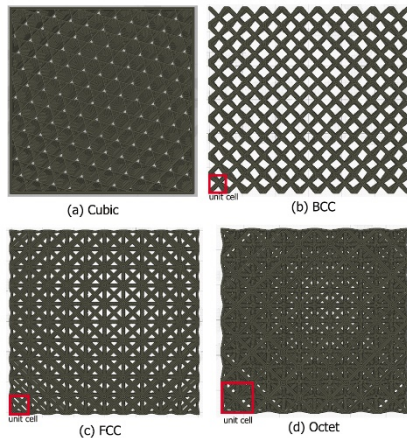


Figure 5 The unit cell of BCC Strut-Base Lattice Structure

In Figure 6., the weight of each sample including the benchmark with 30% infills is shown in simulation using CURA slicing software. It clearly shows that each sample has matched the weight of the benchmark. Therefore, the samples with the proposed infill pattern are proven to have a 30% infill density. Slicing software saves the entire simulation into a GCODEs file, which the 3D printer reads as a command to print. The samples are printed all together in one batch printing set up as shown in Figure 7. to save the time of preparation and printing.

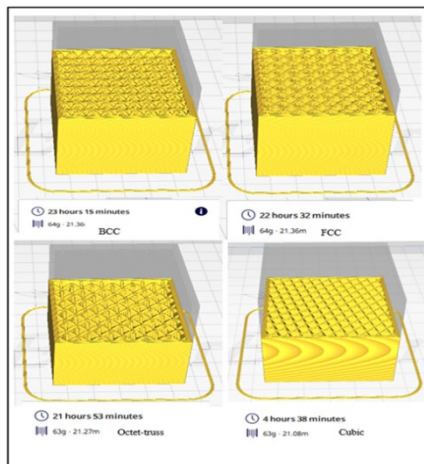


Figure 6 Simulation of samples with lattice infill in Slicing software

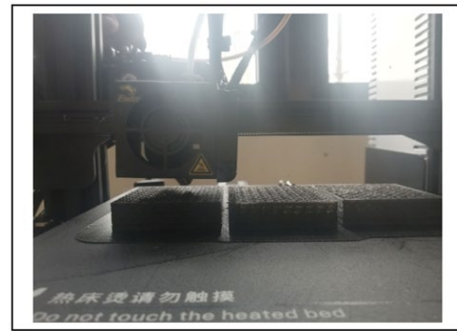


Figure 7 3D printing of testing samples

The printing material used is a black PLA with 1.75 mm diameter as it is one of the most common filaments used in 3D printing. 3D prints occasionally have small plastic strands in places where the printers should not print. It is typically due to the continuous discharging of filaments out of the nozzle while the extruder moves to a new location. These unwanted strands of plastic are called strings. Printing lattice structures eventually creates unwanted strings because of their pattern that frequently moves the extruder from one point to another. To avoid stringing of print, adjusting temperature of the nozzle was a key factor as higher temperature causes the material to become more liquid, allowing it to drip easily from the nozzle. The material is less liquid and thus less likely to string when heated to a lower temperature. So, the temperature of the printing nozzle was set into an ideal setting of 180°C at 50 mm/s printing speed as per recommended in [19]. In Figure 8., the 3D printed testing samples are weighed using an analytical scale to verify the uniformity in weight of the samples in which the samples weigh 54.96g to 55.7 g. Then, using a Chenda universal testing machine, compressive testing was done between two parallel metal plates, as illustrated in figure 9. A regulated displacement value was used to drive the hydraulic heads, and output data for concurrent force and displacement were logged wherein in every 0.1 second, force and displacement were measured. The compression rate was a 1 mm/min ramp input up to a total displacement of 25 mm [20].

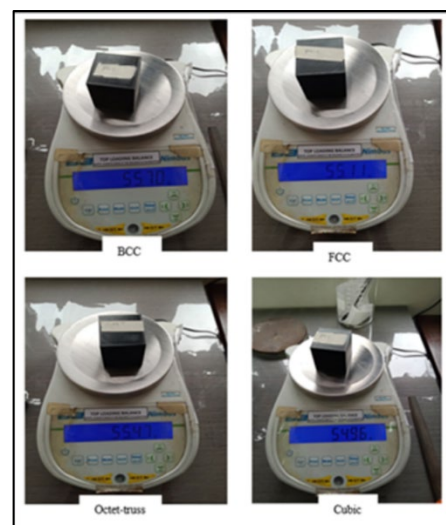


Figure 8 Weighing of test samples using analytical balance



Figure 9 Compressive Test using UTM

### 3.0 RESULTS AND DISCUSSION

Each sample of 3D printed object with lattice infills including the benchmark infills were printed with 30% infill density and consumes an average amount of 55.3 g of PLA filament. Each sample undergo in similar compression load test.

The experimental results obtained were shown in Figures 10 and 11 for the compressive modulus and the stress-strain curve. Based on the curve behavior of the compression test, The FCC, Octet-truss, and Cubic have similar trends in the elastic region except for the BCC lattice, which has higher displacement in a lesser amount of load. Several drops or a fluctuation of curves in all samples can also be seen before reaching a higher load; this indicates that the weak layers of infill are fractured layer by layer since the infills are made out of multiple layered units' cells. Furthermore, the FCC and Octet-truss have very similar behavior in their elastic region directly upon the fluctuation in the initial displacement of 5 mm while BCC endures more strain at minimal load from the beginning up to 26 mm of displacement and then exhibit rise of the slope after several drops. It can also be seen in the stress-strain curve that the BCC, FCC, and Octet-truss have a stiffer curve in the elastic region, neglecting the initial stage before the fluctuation. The specific strength of each testing sample was calculated, and the results are shown in Figure 11, wherein BCC has the highest compressive strength of 11.25 MPa, followed by the benchmark Cubic infill with 9.73 MPa, FCC with 8.47 MPa, and last Octet-truss with 7.44 MPa. Comparing the compressive strength of the proposed lattice infill with benchmark samples, one of the samples (BCC) yields higher compressive strength than the benchmark infill.

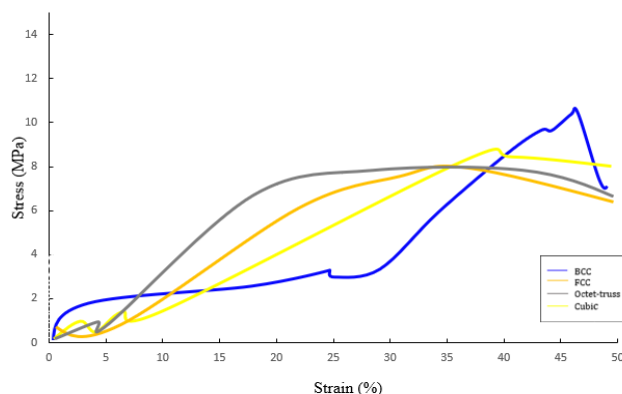


Figure 10 The stress-strain curve of 3D printed samples with lattice infills and cubic infill as benchmark.

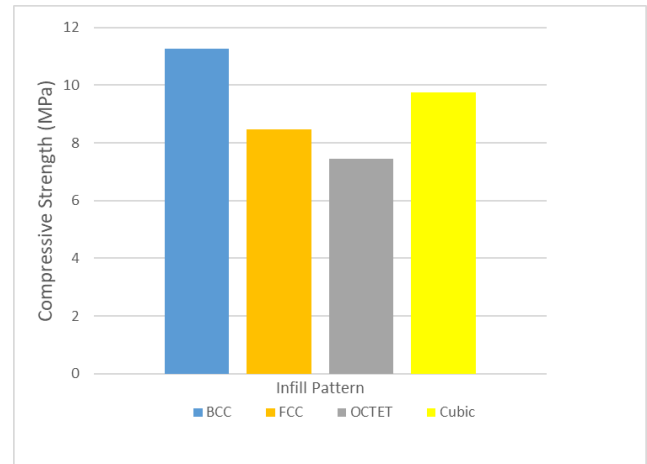


Figure 11 The comparison of compressive strength between 3D printed samples with lattice infills and cubic infills as benchmark.

### 4.0 CONCLUSION

3D printers are programmed to fill fraction of the interior volume of the printed object. This results in a semi-hollow final print which decreases printing time, material consumption, and production costs. As the structure of the infill pattern affects the mechanical properties of the printed part, in this work, innovative infill patterns inspired by strut-base lattice were used as an infills pattern that is stronger and more material-efficient than conventional 3D printing infill. This research provides the design, analysis, and comparison of mechanical strength of the proposed infill pattern to the benchmark infills from slicing software. Three 3D printed lattice infill patterns were analyzed namely: body-centered cubic (BCC), Face-centered cubic (FCC), and Octet cubic. The proposed 3D printed infill undergoes compressive testing by compressing 50.8 mm cubical blocks filled with innovated infill pattern and compared to the default 3D printer infill (cubic). Each block has a different number of lattice cells per sample to comply with the 30% infill density; 870 cells, 641 cells, and 266 cells for BCC, FCC and Octet-truss consecutively. Based on the experimentation, the results showed that the BCC has compressive strength of 11.25 MPa, followed by the benchmark Cubic infill with 9.73 MPa, FCC with 8.47 MPa, and last Octet-truss with 7.44 MPa. With a higher number of units cells the specimen consists of resulted in a higher stress allocation, as more overall struts are available. The results show that the BCC infill pattern has the highest compressive strength among the testing samples. Furthermore, all proposed infill patterns show an increase in stiffness as the modulus of elasticity increases compared to the benchmark. These concludes that the proposed design of a new strut-base lattice infill pattern increases the mechanical properties of the printed object while consuming an equal amount of material to those printed using the default infill pattern.

Printing lattice patterns was quite difficult for the present 3D printers due to their vertical structure; as a result, lattice infill has a longer printing time than the benchmark infill pattern. Moreover, the researcher recommends further research on different printing techniques, which may involve printing orientation, G-code programming to eliminate the use

of third-party software in making Lattice infill and optimize the printing path to improve printing time which allows the proposed infill structure to print at the same time as the default infills.

### Acknowledgement

The Authors would like to express gratitude to the technical and support staff of the Mechanical Engineering Department of De La Salle University for the help they provided.

### References

- [1] Bates-Green, T., Howie, K., 2017. Materials for 3D Printing by Fused Deposition. *Technical Education in Additive Manufacturing & Materials*. 1–21.
- [2] Wang, X., Jiang, M., Zhou, Z., Gou, J., Hui, D., 2017. 3D Printing of polymer matrix composites: A review and prospective. *Composites B*; 110: 442–58. DOI: <http://dx.doi.org/10.1016/j.compositesb.2016.11.034>,
- [3] Ngo, T.D., Kashani, A., Imbalzano, G., Nguyen, K.T., Hui, D., 2018. Additive manufacturing (3D printing): A review of materials, methods, applications and challenges. *Composites B*; 143:172–96. DOI: <http://dx.doi.org/10.1016/j.compositesb.2018>.
- [4] Bandar, A., Subbarayan, S., Ammar M., 2020. Investigation of infill-patterns on mechanical response of 3D printed poly-lactic-acid. *Polymer Testing*. 87. DOI: <https://doi.org/10.1016/j.polymertesting.2020.106557>.
- [5] Aloyaydi, B.A., Sivasankaran, S., Ammar, H.R., 2019. Influence of infill density on microstructure and flexural behavior of 3D printed PLA thermoplastic parts processed by fusion deposition modeling. *AIMS Materials Science* 6: 1033. DOI: <https://doi.org/10.3934/mat.2019.6.1033>
- [6] Johnson, G. A., French, J. J., 2018. Evaluation of Infill Effect on Mechanical Properties of Consumer 3D Printing Materials. *Advances in Technology Innovation*. 3(4): 179–184,
- [7] Farbman, D., McCoy, C., 2016. Materials testing of 3D printed ABS and PLA samples to guide mechanical design. *ASME 2016 11th International Manufacturing Science and Engineering Conference 2016*, 2. DOI: 10.1115/MSEC2016-8668.
- [8] Wu, J., Aage, N., Westermann, R., Sigmund, O., 2018. Infill Optimization for Additive Manufacturing—Approaching Bone-Like Porous Structures. *IEEE Transactions on Visualization and Computer Graphics*. 24(2): 1127–1140. DOI: 10.1109/TVCG.2017.2655523
- [9] Taf, S.T., Huiskes, R., Ruimerman, R., Van Lenthe, G.H., Janssen, J.D., 2000. Effects of mechanical forces on maintenance and adaptation of form in trabecular bone. *Nature*, 405(6787): 704–706. DOI: <https://doi.org/10.1038/35015116>
- [10] Ni, Y., Wang, L., Fan, Y., 2017. Mechanical Properties of Triply Periodic Minimal Surface Structures Mimicking the Microstructure of Woodpecker's Cranial Bone., 2017. *39th Annual International Conference of the IEEE Engineering in Medicine and Biology Society (EMBC)*. 1873-1876, DOI:10.1109/EMBC.2017.8037212.
- [11] [11] Chu, T., Damirez, V.E., Ramos, L., Venancio, L., Chua, A., 2020. Increasing Material Efficiency of Additive Manufacturing through Lattice Infill Pattern. *International Journal of Automation and Smart Technology*. 10: 101-108. DOI:10.5875/ausmt.v10i1.2140.
- [12] Hao, L., Raymont, D., Yan, C., Hussein, A., and Young, P., 2012. Design and additive manufacturing of cellular lattice structures. *International Journal of Frontiers in Engineering Technology*, 3(4): 63-69. DOI: <https://doi.org/10.25236/IJFET.2021.030410>.
- [13] Gibson, L. J., 1989. Modelling the mechanical behavior of cellular materials. *Materials Science and Engineering: A*, Volume 110: 1-3. DOI: 10.1016/0921-5093(89)90154-8.
- [14] Ashby, M.F., 2006. The properties of foams and lattices. *Philosophical transactions. Series A, Mathematical, physical, and engineering sciences*, 364(1838): 15–30. DOI: <https://doi.org/10.1098/rsta.2005.1678>
- [15] Maconachie, T., Leary, M., 2019. SLM lattice structures: Properties, performance, applications and challenges. *Materials & Design*, Volume 183: 108137, DOI: 10.1016/j.matdes.2019.108137.
- [16] Pan, Z., Ma, R., Wang, D., Chen, A., 2018. A review of lattice type model in fracture mechanics: theory, applications, and perspectives. *Engineering Fracture Mechanics*. 190: 382–409, DOI: 10.1016/j.engfracmech.2017.12.037.
- [17] Kim, H.J., Song, K.I., Jung, H.S., Shin, Y.W., Shin, J. H., 2018. Performance evaluation of lattice girder and significance of quality control. *Tunnelling and Underground Space Technology*. 82: 482–492 DOI: 10.1016/j.tust.2018.08.058.
- [18] Deshpande, V.S., Ashby, M.F., Fleck, N.A., 2001. Foam topology: bending versus stretching dominated architectures. *Acta Materialia*, 49(6): 1035–1040. DOI: 10.1016/S1359-6454(00)00379-7.
- [19] Yao, T., Deng, Z., Zhang, K., Li, S., 2019. A method to predict the ultimate tensile strength of 3D printing polylactic acid (PLA) materials with different printing orientations, *Composites Part B: Engineering*, 163: 393–402. DOI: 10.1016/j.compositesb.2019.01.025.
- [20] Syam, W.P., Jianwei, W., Zhao, I., Maskery, I. Leach, R., 2018. Design and analysis of strut-based lattice structures for vibration isolation. *Precision Engineering*, 52(September): 494–506. DOI: 10.1016/j.precisioneng.2017.09.010.